HELVETICA
chimica acta

Supporting Information

DFT Simulations as Valuable Tool to Support NMR Characterization of Halide Perovskites: the Case of Pure and Mixed Halide Perovskites

Claudio Quarti,* Eric Furet, and Claudine Katan

DFT simulations as valuable tool to support NMR characterization of halide perovskites: the case of pure and mixed halide perovskites

Claudio Quarti,*[a,b] Eric Furet,[a] and Claudine Katan [a]

[a] Univ Rennes, ENSCR, INSA Rennes, CNRS, ISCR (Institut des Sciences Chimiques de Rennes) - UMR 6226, F 35000 Rennes, France.

[b] University of Mons, Laboratory for Chemistry of Novel Materials, B-7000 Mons, Belgium.

e-mail : claudio.quarti@umons.ac.be

For the 75th anniversary of Prof. Michael Grätzel

Supplementary Material

Assessments on computational parameters: ^{1}H and ^{13}C signals in tetramethylsilane

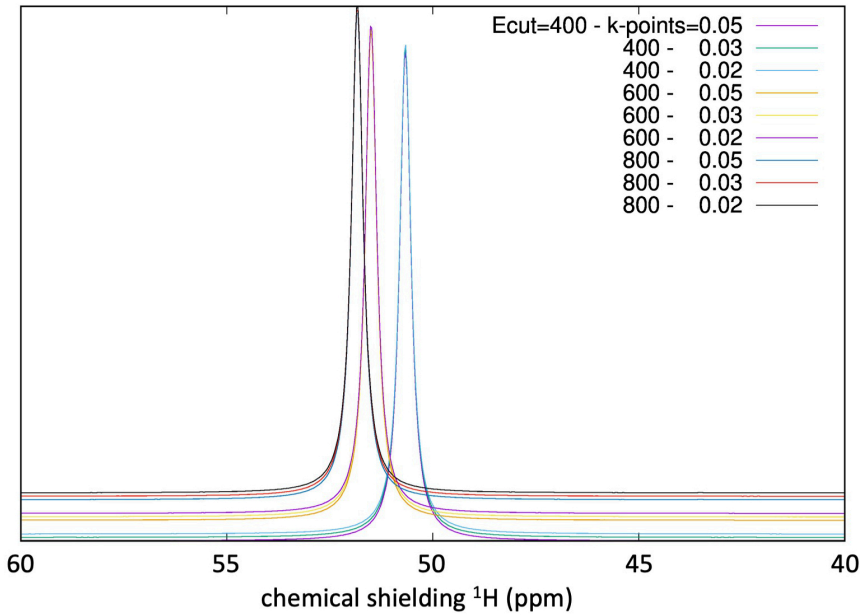

Figure S1. Computed MAS NMR chemical shielding for ^{1}H nuclei in tetramethylsilane, as predicted using different kinetic energy cutoffs (400 eV, 600 eV, 800 eV) and k-point sampling densities for the first Brillouin zone (0.05 $Å^{-1}$, 0.03 $Å^{-1}$, 0.02 $Å^{-1}$).

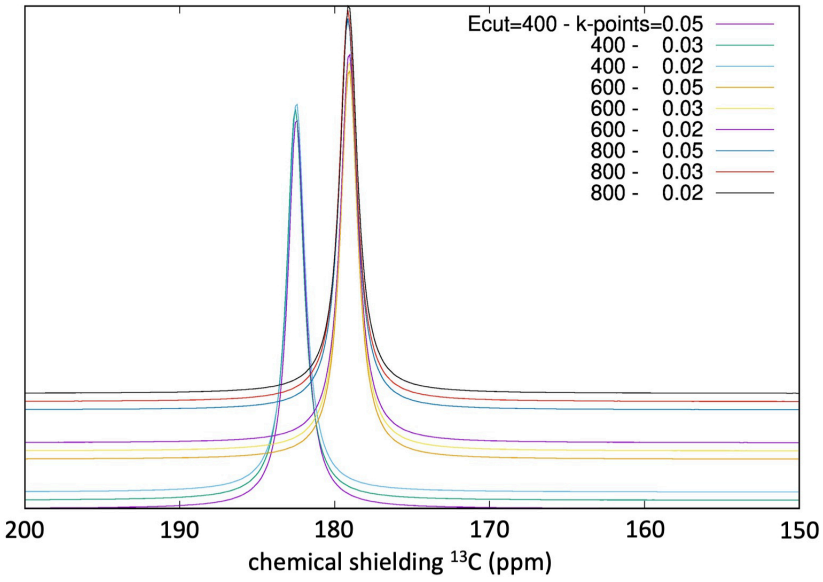

Figure S2. Computed MAS NMR chemical shielding for ^{13}C nuclei in tetramethylsilane, as predicted using different kinetic energy cutoffs (400 eV, 600 eV, 800 eV) and k-point sampling densities for the first Brillouin zone (0.05 $Å^{-1}$, 0.03 $Å^{-1}$, 0.02 $Å^{-1}$).

Assessments on computational parameters: ^{207}Pb in $Pb(NO_2)_3$

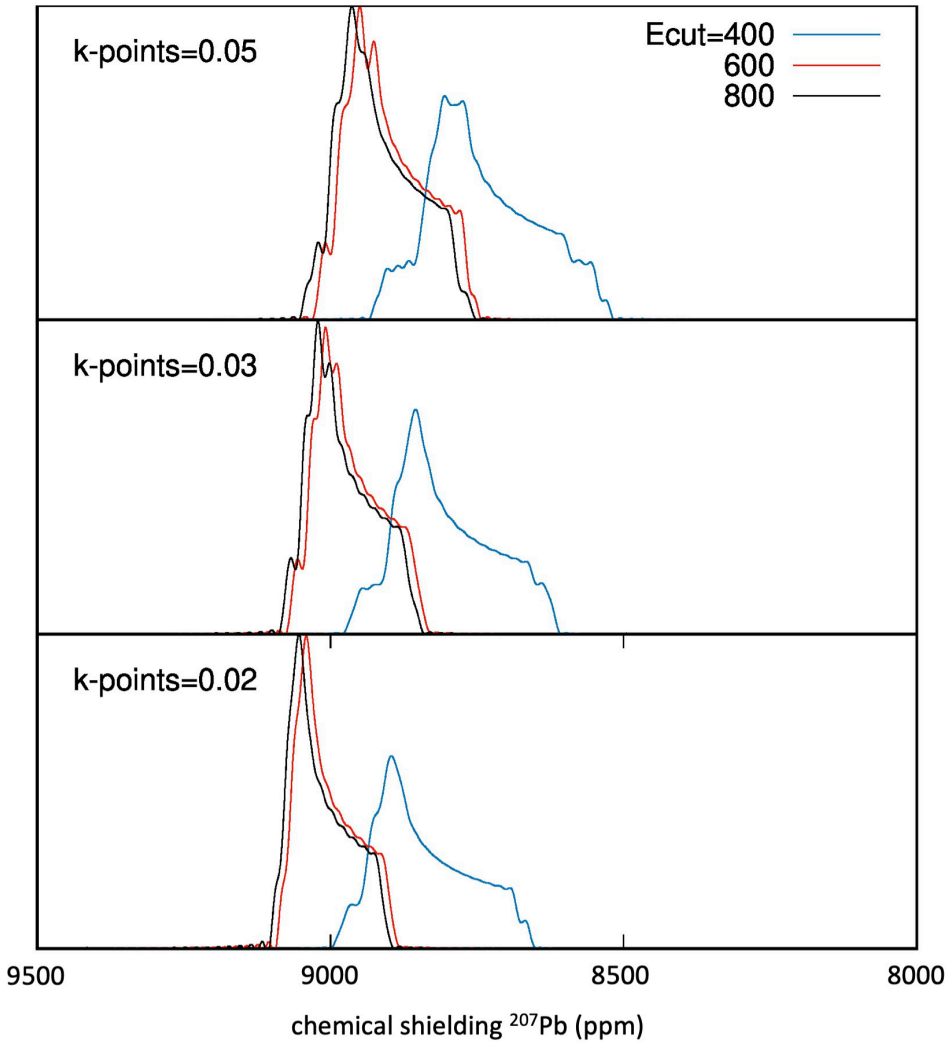

Figure S3. Computed static NMR chemical shielding for ^{207}Pb nuclei in $Pb(NO_2)_3$, as predicted using different kinetic energy cutoffs (400 eV, 600 eV, 800 eV) and k-point sampling densities for the first Brillouin zone (0.05 $Å^{-1}$, 0.03 $Å^{-1}$, 0.02 $Å^{-1}$).

Assessments on computational parameters: ^{1}H, ^{13}C and ^{207}Pb signals in the orthorhombic phase of $CH_3NH_3PbBr_3$ ($MAPbBr_3$)

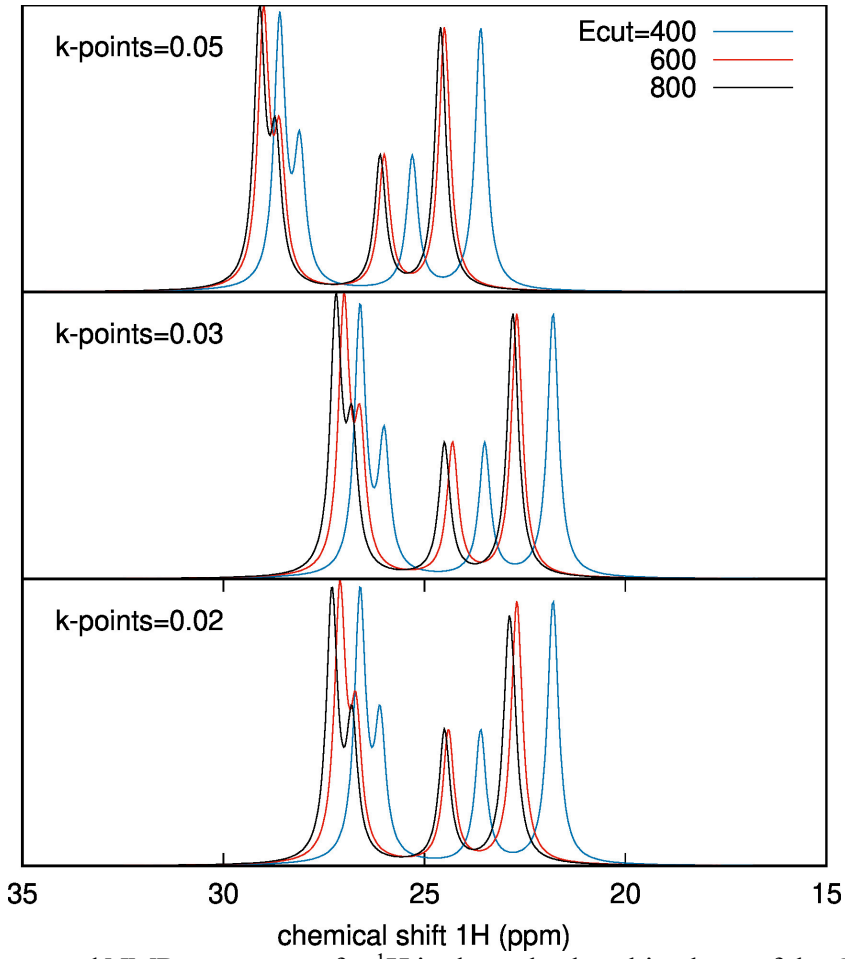

Figure S5. Computed NMR parameters for ^{1}H in the orthorhombic phase of the $CH_3NH_3PbBr_3$, as predicted using different kinetic energy cutoffs (400 eV, 600 eV, 800 eV) and k-point sampling densities for the first Brillouin zone (0.05 $Å^{-1}$, 0.03 $Å^{-1}$, 0.02 $Å^{-1}$). The broadening parallels the conditions of MAS measurement.

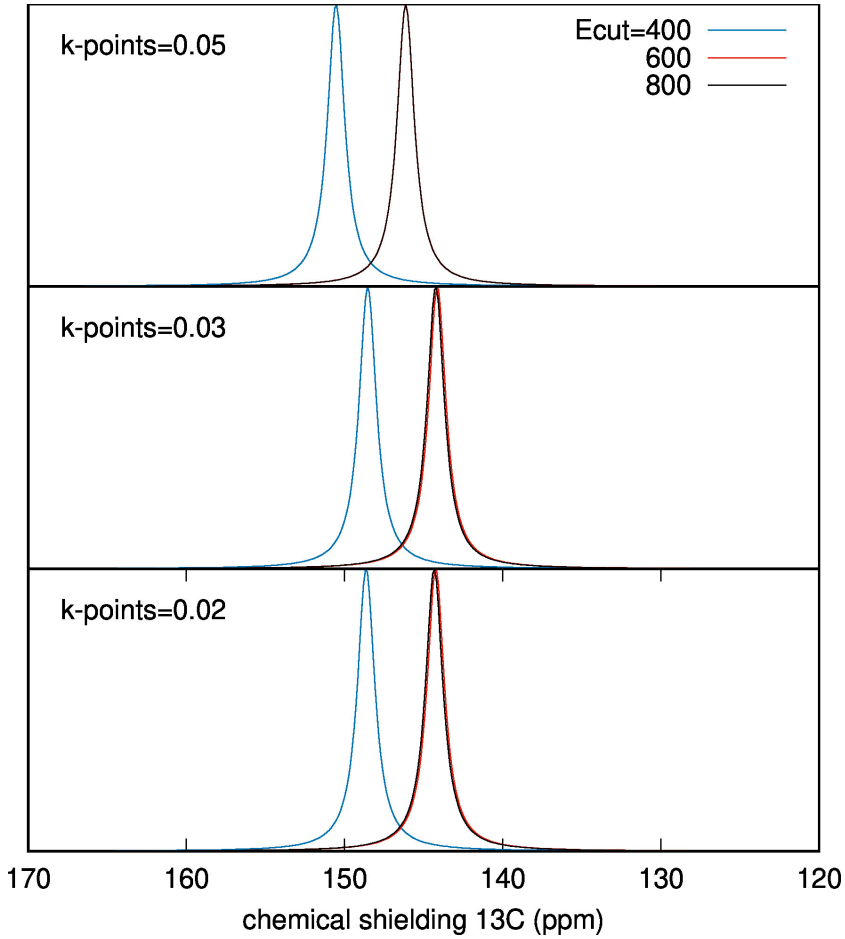

Figure S5. Computed NMR parameters for ^{13}C in the orthorhombic phase of the $CH_3NH_3PbBr_3$, as predicted using different kinetic energy cutoffs (400 eV, 600 eV, 800 eV) and k-point sampling densities for the first Brillouin zone (0.05 $Å^{-1}$, 0.03 $Å^{-1}$, 0.02 $Å^{-1}$). The broadening parallels the conditions of MAS measurement.

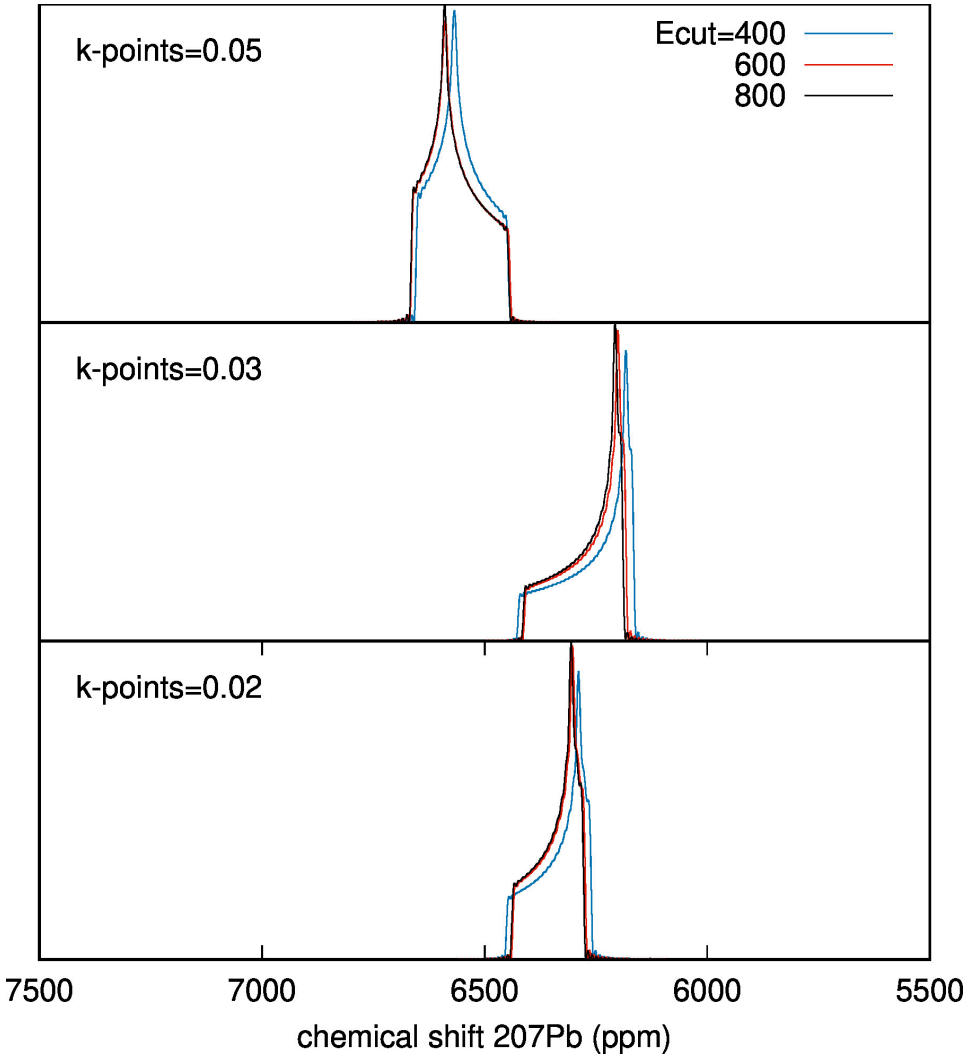

Figure S6. Computed NMR chemical shielding for ^{207}Pb nuclei in the orthorhombic phase of the $CH_3NH_3PbBr_3$ perovskite, as predicted using different kinetic energy cutoffs (400 eV, 600 eV, 800 eV) and k-point sampling densities for the first Brillouin zone (MP=0.05 $Å^{-1}$, 0.03 $Å^{-1}$, 0.02 $Å^{-1}$). The broadening parallels the conditions of MAS measurement and the CSA, as due to the use of zero Kelvin frozen structure.

Calculation of NMR chemical shielding on known dataset for the determination of the proper definition of the chemical shift of ^{1}H, ^{13}C and ^{207}Pb nuclei

Below, we list the reference compounds for the construction of Figure 2 with related literature references for the experimental isotropic shifts, crystalline structures and computed NMR parameters. All periodic calculations have been performed using periodic DFT calculations, adopting our reference computational set-up (600 eV cutoff for the kinetic energy and 0.03 $Å^{-1}$ for the k-point sampling).

Table S1. Dataset for the determination of the chemical shift in for ^{1}H nuclei. Crystal structures and reference experimental data are taken from Ref. [1]

compound	experimental δ_{iso} (ppm)	periodic DFT σ_{iso} (ppm)
COYRUD11	7.0	22.8
	6.1	24.2
	5.9	24.8
	4.5	25.7
	4.1	26.2
	3.8	26.6
	3.2	27.1
	2.3	27.9
	1.8	28.6
FLUBIP	0.9	29.9
	2.9	28.8
	6.7	24.9
BAPLOT01	14.6	14.4
	7.7	22.8
	3.4	27.1
INDMET	7.3	23.0
	7.3	23.1
	7.2	23.1
	6.1	24.1
	5.8	24.4
	5.8	24.6
	5.7	27.2
	2.2	28.2
	1.8	29.2
	1.7	29.3

Table S2. Dataset for the determination of the chemical shift in for ^{13}C nuclei. Crystal structures and reference experimental data are taken from Ref. [1]

compound	experimental δ_{iso} (ppm)	periodic DFT σ_{iso} (ppm)
NAPHTA36	134.9	37.1
	129.9	40.4
	129.3	40.4
	126.0	40.8
	125.4	45.2
GLYCIN03	176.2	-7.5
	43.5	130.0
PERYTO10	58.4	111.4
	50.2	120.24
LTYROS11	176.0	-6.5
	155.7	12.0
	131.0	39.6
	130.3	39.9
	123.0	48.4
	117.2	52.7
	117.2	54.2
	54.7	114.7
	35.8	134.3

Table S3. Dataset for the determination of the chemical shift in for ^{207}Pb nuclei. Reference experimental data are taken from Ref. [2], while list of crystal structures can be found in Ref.[3].

compound	experimental δ_{iso} (ppm)1939	periodic DFT σ_{iso} (ppm)
$Pb(NO_3)_2$	-3494	8994
α-Pb	1939	5833
β-Pb	1515	6003
Pb_3O_4	-1105	6462
	795	6044
PbF_2	-2667	8262
$PbCl_2$	-1717	7664
$Pb_3(PO_4)_2$	-2886	8463
	-2016	8427
$PbSiO_3$	93	7111
	-166	7273
	-366	7350

Results from periodic DFT simulations for ^{13}C nuclei in halide perovskites: computed isotropic chemical shifts and NMR Magic Angle Spinning spectrum for ^{13}C nuclei for the models cubic 1-4 of $MAPbI_3$ and $MAPbBr_3$ perovskites

Table S4. Computed isotropic chemical shifts for ^{13}C nuclei in the various models considered here (see Figure 1 in the main text). Orthorhombic and tetragonal models contain only 4 methylammonium (MA) cations per crystalline cells, hence four Carbon atoms; the supercell models employed to simulate the high temperature cubic phase contain eight Carbon atoms. Data in ppm.

	ortho	tetra	cubic 1	cubic 2	cubic 3	cubic 4
			MAPbI3			
MA 1	27	23	26	30	24	28
MA 2	27	23	26	25	26	31
MA 3	27	23	27	28	26	27
MA 4	27	23	27	28	26	26
MA 5			28	27	27	26
MA 6			28	26	26	26
MA 7			25	26	26	23
MA 8			29	25	28	26
			MAPbBr3			
MA 1	27	25	30	24	25	28
MA 2	27	25	27	27	27	31
MA 3	27	25	25	27	26	29
MA 4	27	25	27	24	27	27
MA 5			27	25	29	28
MA 6			25	26	26	27
MA 7			25	27	26	23
MA 8			29	25	27	27

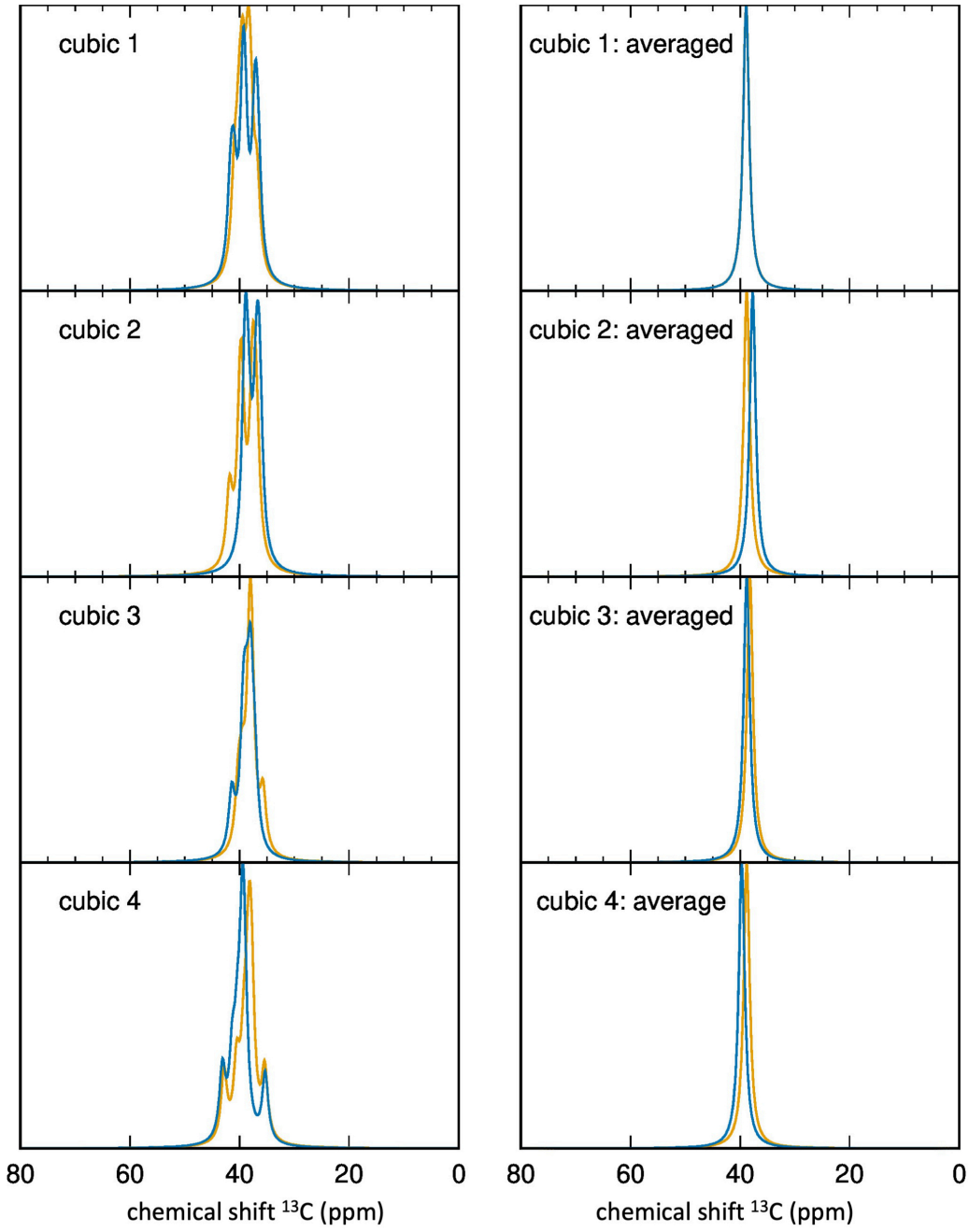

Figure S7. Computed MAS NMR spectra for the ^{13}C nuclei of the cubic 1-4 models used to simulate the high temperature phase of $MAPbI_3$ and $MAPbBr_3$. The left panel corresponds to the NMR spectrum obtained from DFT calculations. The right panel corresponds to the spectrum with the signals from equivalent carbon atoms averaged as proposed in Ref. [4] (see main text).

Results from periodic DFT simulations for ^{207}Pb nuclei in halide perovskites: list of computed isotropic chemical shifts and CSA for the various investigated models

Table S5. Isotropic chemical shifts computed for ^{207}Pb nuclei in the various models considered here (see Figure 1 in the main text). Orthorhombic and tetragonal models contain only 4 lead atoms per crystalline cells; the supercell models employed to simulate the high temperature cubic phase contain eight lead atoms. Data in ppm.

	ortho	tetra	cubic 1	cubic 2	cubic 3	cubic 4
			MAPbI3			
Pb 1	1202	1224	1271	1276	1286	1460
Pb 2	1203	1206	1231	1281	1203	1393
Pb 3	1202	1193	1287	1249	1358	1375
Pb 4	1203	1214	1255	1271	1298	1371
Pb 5			1379	1257	1280	1261
Pb 6			1291	1208	1216	1210
Pb 7			1336	1255	1292	1253
Pb 8			1256	1313	1325	1232
			MAPbBr3			
Pb 1	585	650	718	729	813	838
Pb 2	585	638	735	692	761	784
Pb 3	585	632	759	757	728	739
Pb 4	585	646	758	684	716	735
Pb 5			757	741	785	748
Pb 6			755	747	791	731
Pb 7			811	734	752	751
Pb 8			796	758	784	777

Table S5. Chemical shift Anisotropy (CSA) computed for ^{207}Pb nuclei in the various models considered here (see Figure 1 in the main text). Orthorhombic and tetragonal models contain only 4 lead atoms per crystalline cells; the supercell models employed to simulate the high temperature cubic phase contain eight lead atoms. Data in ppm

	ortho	tetra	cubic 1	cubic 2	cubic 3	cubic 4
			MAPbI3			
Pb 1	274	169	-137	80	-181	-80
Pb 2	274	187	83	164	-55	-85
Pb 3	274	188	215	89	155	100
Pb 4	274	167	-102	107	-191	77
Pb 5			114	-106	-172	229
Pb 6			84	118	-176	218
Pb 7			126	27	-216	182
Pb 8			64	110	216	-177
			MAPbBr3			
Pb 1	-146	84	-148	157	204	-100
Pb 2	-146	92	-114	174	49	-145
Pb 3	-146	81	131	-73	-181	-189
Pb 4	-146	74	143	115	-228	-92
Pb 5			39	154	-181	-183
Pb 6			85	210	-170	171
Pb 7			-107	-75	104	216
Pb 8			-105	128	-115	202

Analysis of halide composition and distribution for the models used to simulate mixed bromine:iodine methylammonium lead perovskites

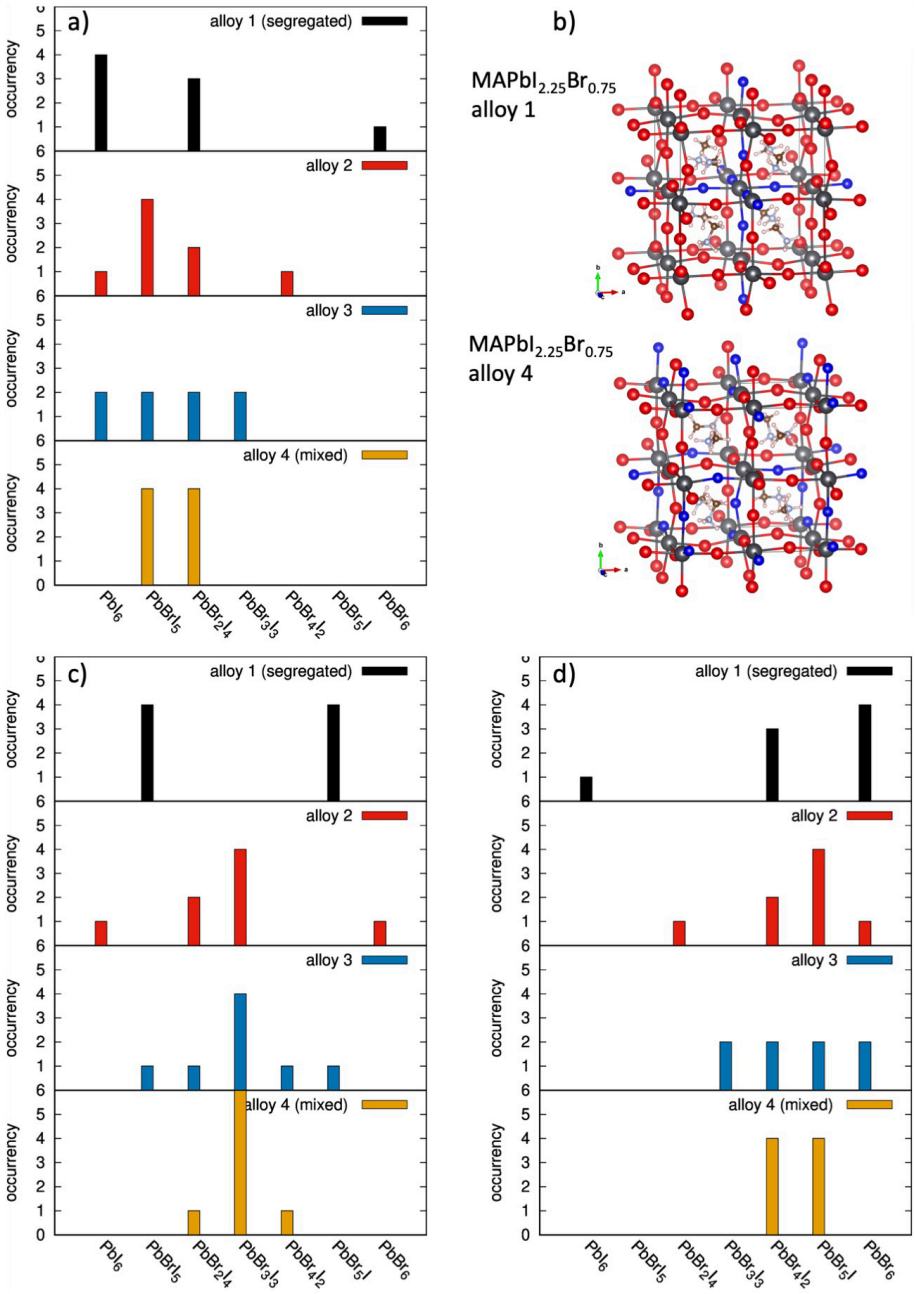

Figure S8. a) number of PbX_6 octahedra with given composition, for the alloy 1 - 4 models employed to simulate the mixed halide perovskite with composition $MAPbI_{2.25}Br_{0.75}$; b) related alloy 1 and alloy 4 models (corresponding to halide segregated and homogeneously distributed model, respectively). Color code is: dark grey=lead, red=iodine, blue=bromine, brown=carbon, light blue=nitrogen, light pink=hydrogen; c-d) number of PbX_6 octahedra with given composition for the alloy 1 - 4 models associated to $MAPbI_{1.5}Br_{1.5}$ (c) and $MAPbI_{0.75}Br_{2.25}$ composition (d).

Correlation between the anisotropic part of the chemical tensor and the octahedral elongation λ_{oct} and deformation σ parameters

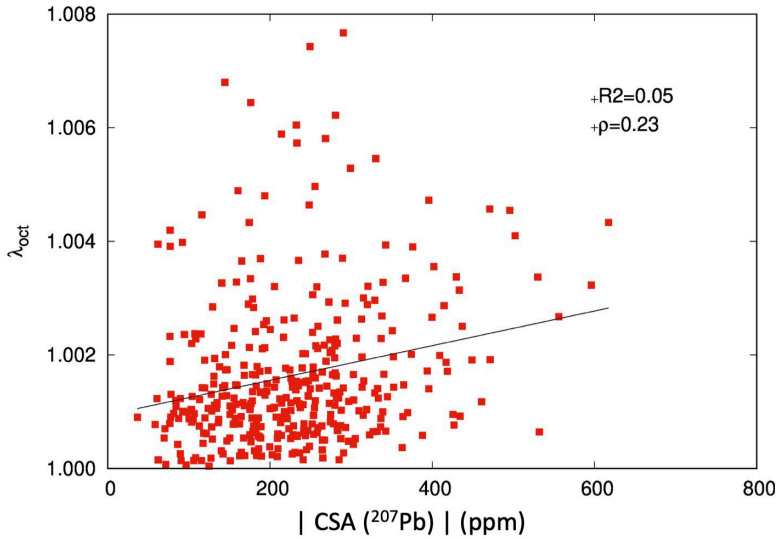

Figure S9. Absolute value of the anisotropic chemical shift computed for 50 snapshots of the dynamic simulations for the cubic model of $MAPbI_3$, as function of the octahedra λ_{oct} (red dots) elongation parameter. Black line represents the best fitting linear function, with corresponding R^2 coefficient and Pearson coefficient (ρ).

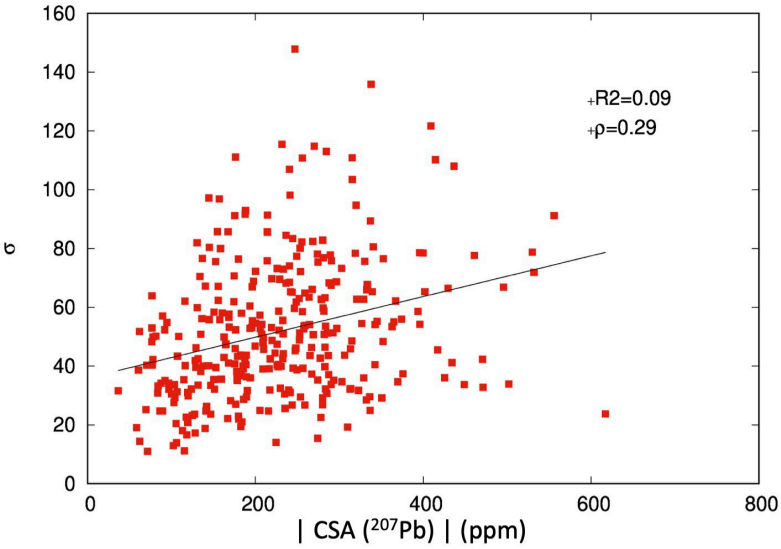

Figure S10. Absolute value of the anisotropic chemical shift computed for 50 snapshots of the dynamic simulations for the cubic model of $MAPbI_3$, as function of the octahedra λ_{oct} (red dots) elongation parameter. Black line represents the best fitting linear function, with corresponding R^2 coefficient and Pearson coefficient (ρ).

References

[1] J. D. Hartman, R. A. Kudla, G. M. Day, L. . J. Mueller, G. O. J. Beran, 'Benchmark fragment-based 1H, 13C, 15N and 17O chemical shift predictions in molecular crystals', *Phys. Chem. Chem. Phys.* **2016**, *18*, 21686–21709.

[2] F. Fayon, I. Farnan, C. Bessada, J. Coutures, D. Massiot, J. P. Coutures, 'Empirical Correlations between 207Pb NMR Chemical Shifts and Structure in Solids', *J. Am. Chem. Soc.* **1997**, *119*, 6837–6843.

[3] F. Alkan, C. Dybowski, 'Chemical-shift tensors of heavy nuclei in network solids: a DFT/ZORA investigation of 207Pb chemical-shift tensors using the bond-valence method', *Phys. Chem. Chem. Phys.* **2015**, *17*, 25014–25026.

[4] J. M. Griffin, S. Wimperis, A. J. Berry, C. J. Pickard, S. E. Ashbrook, 'Solid-State 17O NMR Spectroscopy of Hydrous Magnesium Silicates: Evidence for Proton Dynamics', *J. Phys. Chem. C.* **2009**, *113*, 465–461.